Optical, Magnetic and Electrochemical Properties of Spinel Mn_3O_4, Co_3O_4 Nanostructures

Dr. Dadamiah PMD Shaik[1], Associate Professor,
Dept. of Physics, Vardhaman College of Engineering,
Hyderabad, Telangana-501218

Dr. Md Sameer Ahmed[2,] Associate Professor,
Dept. of Chemistry, Lords Institute of Engg & Tech.
Hyderabad, Telangana-500091

ABSTRACT

Manganese oxide (Mn_3O_4) and Cobalt oxide (Co_3O_4) nanocrystals were synthesized using a straightforward and cost-effective combustion method. Structural analysis through XRD, Raman Spectroscopy, and Fourier Transform Infrared Spectroscopy confirmed the tetragonal structure with I41/amd (141) space group for Mn_3O_4 and the cubic structure with Fd3m (227) space group for Co_3O_4. The average crystallite sizes were determined using the Debye Scherer formula, resulting in approximately 14 nm for Mn_3O_4 and 22 nm for Co_3O_4. SEM images displayed irregular and uniform spherical grains for Mn_3O_4 and Co_3O_4, respectively, with average grain sizes of 100 nm and 120 nm. EDS and XPS spectra showed clear binding energy peaks for Manganese, Cobalt, and Oxygen, confirming the chemical purity of the samples. The optical band gap of the nanocrystals was found to be 2.93 eV for Mn_3O_4 and 2.50 eV for Co_3O_4. Magnetic analysis revealed a strong ferromagnetic nature at 5 K temperature for both Mn_3O_4 and Co_3O_4 nanocrystals. Electrochemical investigations demonstrated that Mn_3O_4 nanocrystals exhibited excellent performance as electrodes for electrochemical capacitors. At a current density of 0.5 A g^{-1}, they achieved a high specific capacitance of 417 F g^{-1}, maintaining almost 100% coloumbic efficiency after 600 cycles and displaying good cyclic stability for up to 10,000 cycles. On the other hand, Co_3O_4 showed inferior electrochemical behavior, indicating that Mn_3O_4 nanocrystals possess superior mass transport of electrolyte ions into the electrode, making them more suitable for electrochemical capacitors.

Keywords—Spinel Mn_3O_4 and Co_3O_4 nanocrystals, band gap, specific capacitance, cyclability.

I. INTRODUCTION

In recent times, electrochemical capacitors have emerged as promising energy storage devices due to their advantageous characteristics, such as long cycle life, high energy, and power densities [1]. Previous research indicates that the choice of electrode material and electrolyte significantly influences the performance of supercapacitors. Transition metal oxides and conducting polymers are commonly used as active electrode materials, providing high capacitance but poor cycling performance due to faradaic redox reactions [2, 3]. Alternatively, carboneous electrodes offer better cyclability but lower capacitance, relying on double-layer capacitance between the electrode and electrolyte.

Among transition metal oxides, some like Ru_2O, MoO_3, V_2O_5, Fe_2O_3, Mn_3O_4, CuO, ZnO, MnO_2, Co_3O_4, NiO, and TiO_2 have received extensive attention for their high theoretical specific capacitance [4, 5]. Among these, RuO_2 is well-studied for its high conductivity, specific capacitance, and chemical stability.

However, its limited abundance and high cost hinder practical applications. Spinels like Mn_3O_4 and Co_3O_4 are considered attractive electrode materials due to their cost-effectiveness, eco-friendliness, and intrinsic high capacity [6-11]. These materials find applications in various fields, including rechargeable lithium-ion batteries, molecular adsorption, electrochemistry, magnetism, and supercapacitors. Additionally, they are utilized in oxygen reduction and reaction (ORR) catalysis due to their excellent catalytic abilities in ORR. Moreover, the unique magnetic properties of these nanoparticles have garnered attention for potential applications in data storage, magnetic particle imaging, wastewater treatment, and more [13, 14].

Spinel ferrites and their composites have also found applications in diverse areas, thanks to their unusual magnetodielectric properties. For example, substituted spinel ferrites synthesized through various methods have been utilized in anti-cancer and functional radio electronic devices, catalysis, and biological applications [15-20].

However, there is limited research comparing the magnetic and electrochemical properties of spinel Mn_3O_4 and Co_3O_4 nanocrystals prepared via combustion synthesis. While various methods exist for synthesizing oxide nanoparticles, combustion synthesis stands out due to its simplicity, low temperature, and short processing time. This article aims to investigate and compare the optical, magnetic, ac capacitance, and electrochemical properties of spinel Mn_3O_4 and Co_3O_4 nanocrystals. The study reveals that Mn_3O_4 nanocrystals outperform Co_3O_4, attributed to their high spin and suitable structure with a smaller crystallite size [23, 24].

II. EXPERIMENTAL PROCEDURE

The reagents utilized in synthesizing spinel Mn_3O_4 nanocrystals were provided by the Merck Company and possessed a purity level of over 99%. The preparation involved using manganese nitrate as the oxidant and urea as the fuel, mixed in a 1:1 molar ratio. The oxidant and fuel mixture was dissolved in 30 ml of deionized water and stirred for approximately 30 minutes using a magnetic stirrer. The resulting solution was collected in a quartz crucible and then placed inside a preheated muffle furnace set at 300 ºC for a duration of 30 minutes. After the chemical reaction was complete, the final product was allowed to cool naturally to room temperature and carefully collected. The detailed step-by-step procedure for the solution combustion technique used to prepare Mn_3O_4 nanocrystals is depicted in the accompanying flowchart. The same experimental procedure was replicated for the synthesis of Co_3O_4 nanocrystals.

.

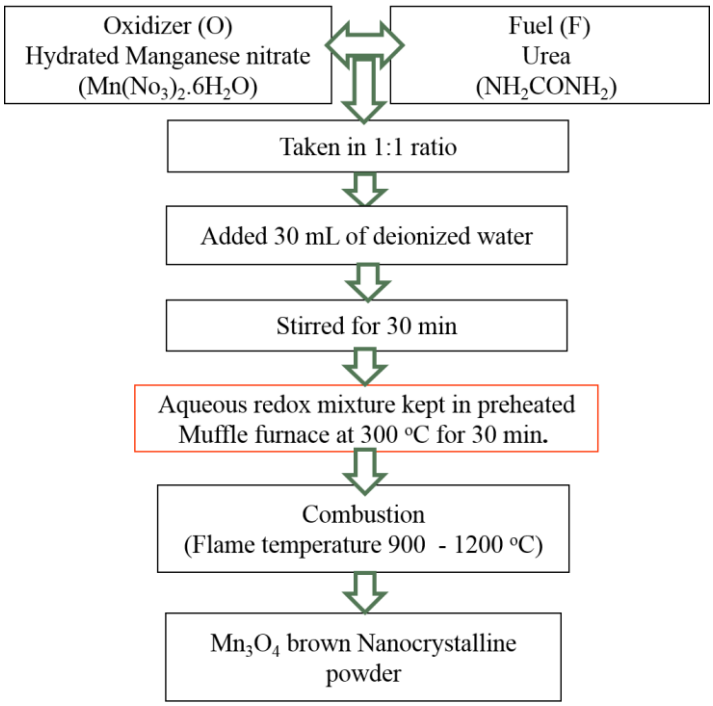

Schematic diagram of solution combustion technique

A. Material Characterization

The structural characteristics of the prepared spinel Mn3O4 and Co3O4 nanocrystals were analyzed using X-ray power diffractometer (XRD-Model 3003 TT) and Raman spectrometer (Horiba Jobin Yvon Lab RAM HR800UV). The vibrational modes of the samples were determined using Fourier Transform Infra-red spectrometer (FTIR-ALPHA interferometer, Bruker). Morphological and elemental analysis of the samples were examined using Scanning Electron Microscopy (SEM) and Energy Dispersive Spectroscopy (EDS) (Carl ZEISS Model EVO MA15).

To perform chemical state analysis, X-ray Photo Electron Spectrometer (XPS) was utilized. The survey and core-level high-resolution spectra were measured with a monochromatic Al Kα X-ray (1486.6 eV) at a vacuum level of 10−9 Torr, an applied beam current of 9 mA, and an acceleration voltage of 13 keV (117 W). The optical band gap of the nanocrystals was investigated using a UV-Vis spectrometer.

For studying the magnetic properties, Vibrational Sample Magnetometer (VSM) was employed. The electrochemical characteristics of the nanocrystals were evaluated through Cyclic Voltammetry (CV), Chronopotentiometry (CP), and Electrochemical Impedance Spectroscopy (EIS) investigations, which were performed using a 608CHI electrochemical analyzer.

B. Electrode preparation

To fabricate the electrode, a mixture of synthesized Mn_3O_4, carbon black, and PVdF in a ratio of 80:10:10 is ground for half an hour. The resulting mixture is then combined with N-methyl-2-pyrrolidone solvent to create a slurry. Using a brush, the slurry is coated onto a chemically cleaned Nickel foam substrate. The coated electrode is subsequently dried in air at 100 °C for a duration of 2 hours.

For the electrochemical performance evaluation of the synthesized Mn_3O_4 nanocrystals, a glass cell is assembled with a working electrode containing the synthesized Mn_3O_4, a platinum foil as the reference electrode, and Ag/AgCl as the counter electrode. The cell is filled with a 1M Na_2SO_4 aqueous solution. The same procedure is followed for preparing the Co_3O_4 nanocrystal electrode for further examination

III. RESULTS AND DISCUSSION

A. Microstructural Properties

The X-ray powder diffraction (XRD) technique was employed to analyze the structure of the synthesized Mn_3O_4 and Co_3O_4 nanocrystals within the range of 10°-70° Bragg's angle. Figure 1a displays the XRD pattern of Mn_3O_4, revealing diffraction peaks at 19.43°, 33.48°, 38.18°, 44.33°, 49.83°, 59.06°, 60.68°, and 64.96°, corresponding to (101), (103), (004), (220), (105), (321), (224), and (440) reflections, respectively. Additionally, a predominant (211) orientation peak was observed at 2θ = 36.3°. These characteristic peaks confirm that Mn_3O_4 possesses a tetragonal structure with I41/amd (141) space group, as identified by the JCPDS card No.89-4837. The lattice parameters are determined as a = b = 5.763 Å and c = 9.456 Å [15]. The high intensity and broadness of these peaks indicate a high degree of crystallinity with a relatively smaller crystallite size.

Figure 1b illustrates the XRD pattern of Co_3O_4, which exhibits a predominant (311) orientation peak at 2θ = 37.19°, along with other characteristic peaks at 31.54°, 38.68°, 44.59°, 55.31°, 59.55°, and 65.35° corresponding to (220), (222), (400), (422), (333), and (440) reflections, respectively. All peaks were indexed to the cubic structure with Fd3m (227) space group, indicative of a normal spinel structure, and the estimated lattice constant is a = b = c = 8.072 Å [15].

The Debye-Scherer's formula (1) was used to determine the crystallite size (D) of the samples, resulting in sizes of 14 nm for Mn_3O_4 and 22 nm for Co_3O_4, respectively

$$D = \frac{k\lambda}{\beta \cos\theta} \qquad \text{----} \qquad (1)$$

where k=0.94, λ=1.5406 Å, β=Width of the diffraction peak at half intensity in radian and θ=Bragg angle in degrees.

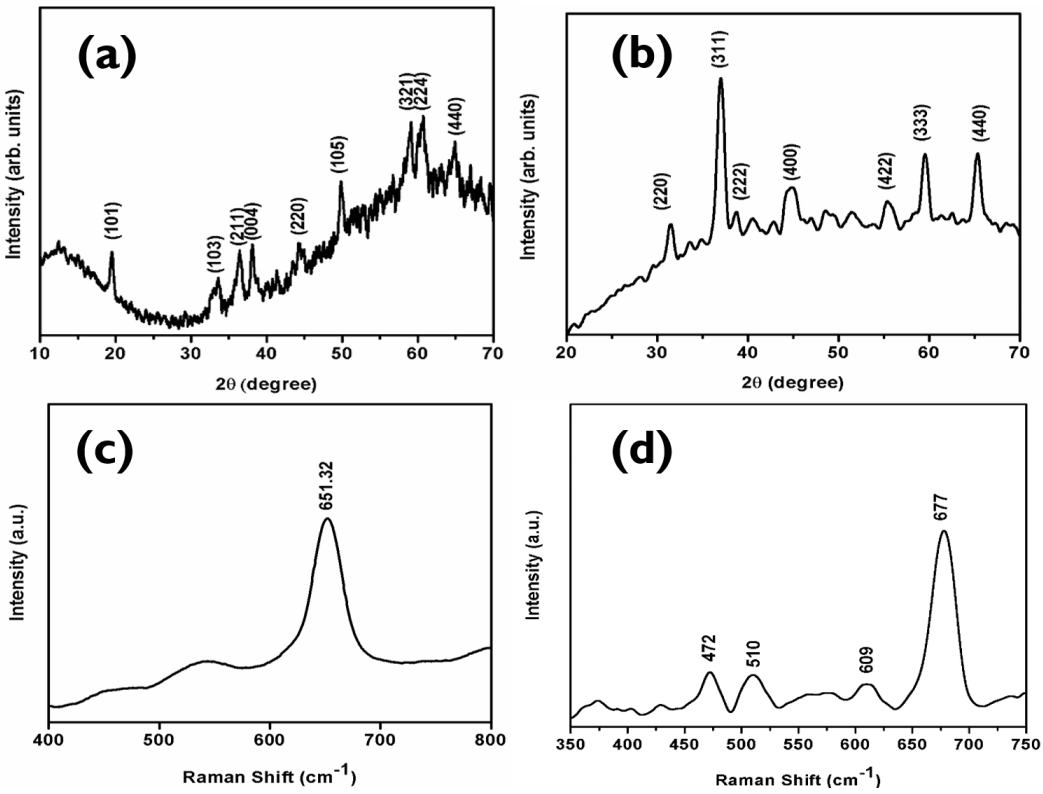

Figure 1: XRD spectra and Raman spectra of spinel a, c) Mn_3O_4, b, d) Co_3O_4 nanocrystals

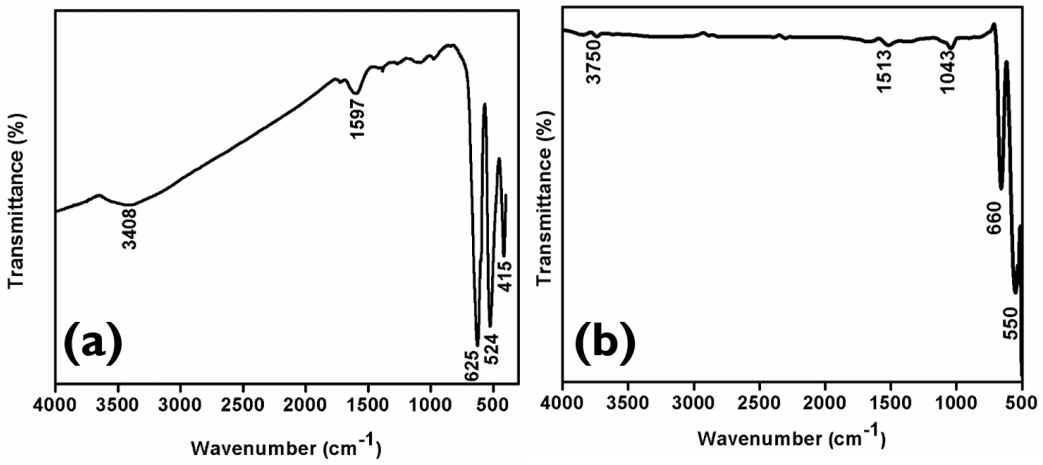

Figure 2: FTIR spectrum of spinel a) Mn_3O_4 b) Co_3O_4 nanocrystals

Raman spectroscopy was employed to confirm the structure of the synthesized Mn_3O_4 and Co_3O_4 nanocrystals. Figure 1c displays the Raman spectrum of Mn_3O_4 in the wavenumber range of 400-800 cm^{-1}. The peak observed at 651.32 cm^{-1} corresponds to the single degenerate A1g symmetry mode, which is attributed to the Mn-O stretching vibrations of Mn^{2+} in tetrahedral coordination [25]. The slight blue shift of this peak indicates a lower crystallite size, supporting the results obtained from XRD [26]. Figure 1(d) shows the Raman spectrum of Co_3O_4 nanocrystals in the Raman shift range of 350-750 cm^{-1}. The strong band around 670 cm^{-1} and a group of weaker intensity bands around 400-600 cm^{-1} are characteristic features of Co_3O_4. The strong peak at 677 cm^{-1} and two weak peaks at 609 and 510 cm^{-1} are attributed to A1g, F2g (1), and F2g (2) vibrations, respectively. These vibrations correspond to Co-O stretching vibrations, Co-O-Co asymmetric stretch, and Co-O

bending modes. Additionally, a faint band at 472 cm^{-1} is identified as Eg, which is a doubly degenerate symmetry mode. These characteristic peaks confirm the cubic structure of Co_3O_4 [27].

FTIR spectra of Mn_3O_4 and Co_3O_4 nanocrystals were recorded in the wavenumber range of 4000-500 cm-1 to analyze the presence of vibrational bonds in the samples (Fig. 2a&b). Figure 2a exhibits absorption peaks at 625 and 524 cm-1, corresponding to the Mn-O stretching mode of tetrahedral and octahedral sites, respectively. Furthermore, a weak absorption peak at 415 cm^{-1} is attributed to the vibration of manganese in an octahedral site. Vibrational bands at 1513 and 3750 cm^{-1} are observed, corresponding to O-H bending vibrations [25]. Figure 2b shows absorption peaks at 550 and 660 cm-1, corresponding to the vibrations of Co^{3+} and Co^{2+} in octahedral and tetrahedral sites, respectively. These FTIR studies confirm the existence of Mn-O and Co-O bonds, further supporting the results obtained from Raman spectroscopy.

The morphology of Mn_3O_4 and Co_3O_4 nanocrystals was examined using Scanning Electron Microscopy (SEM), and the results are shown in Fig. 3. The SEM images reveal that the Mn_3O_4 sample consists of irregularly shaped grains with a non-uniform distribution, having an average size of 100 nm (Fig. 3a&b). Conversely, the Co_3O_4 nanocrystals exhibit a uniform distribution in the form of spherical grains, with an average sphere size of 120 nm (Fig. 3c&d).

To perform elemental analysis, Energy Dispersive Spectroscopy (EDS) was utilized. Figure 3e displays the binding energy peaks of Manganese and Oxygen with atomic percentages of 40.91 and 59.09, respectively. This yields a metal-to-oxygen ratio of 0.69 for the Mn_3O_4 sample. In Figure 3f, the binding energy peaks of Cobalt and Oxygen are shown with atomic percentages of 45.93 and 54.09, respectively, resulting in a metal-to-oxygen ratio of 0.85 for the Co_3O_4 sample. These EDS results confirm the chemical purity of both the Mn_3O_4 and Co_3O_4 samples.

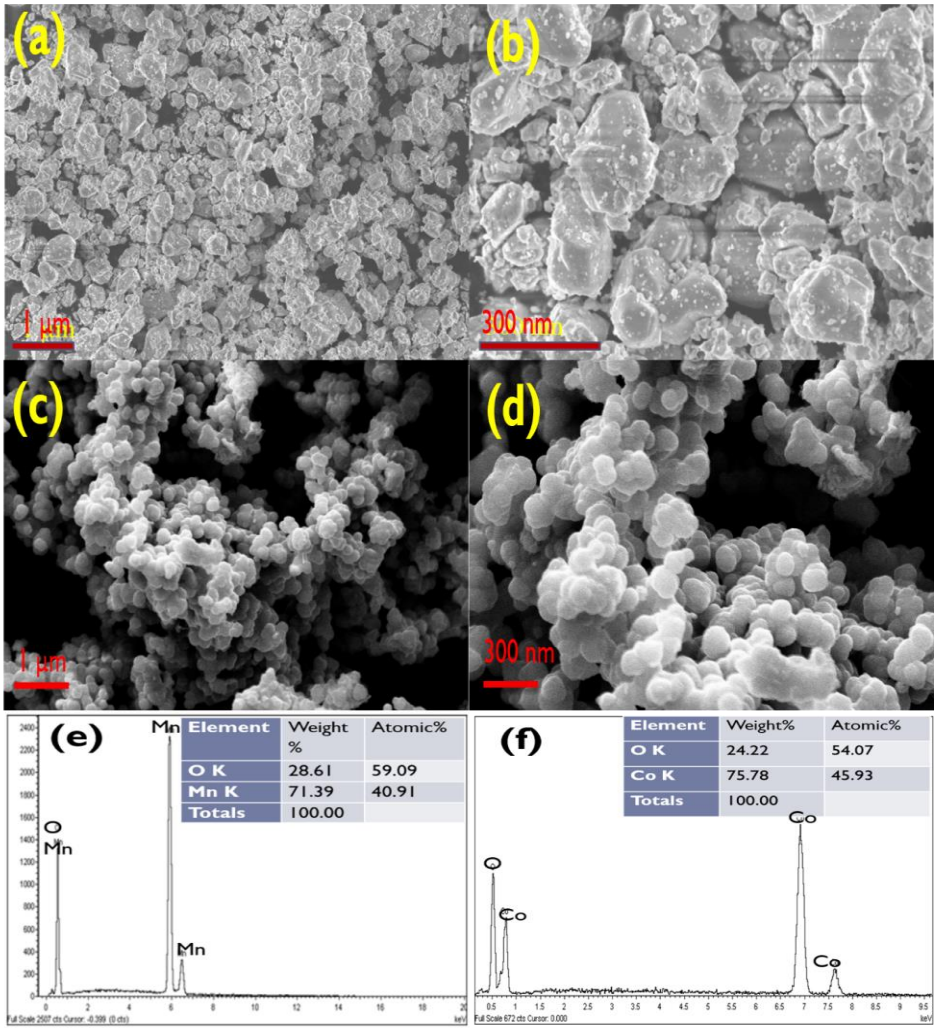

Figure 3: a & b) SEM images of spinel Mn_3O_4 and c & d) Co_3O_4 nanocrystals
EDS of spinel e) Mn_3O_4 f) Co_3O_4 nanocrystals

X-ray Photoelectron Spectroscopy (XPS) studies were conducted to examine the chemical state and composition of the samples. The survey spectrum of the Mn_3O_4 sample contains peaks corresponding to Mn 3p, Mn 3s, O 1s, and Mn 2p, as depicted in Fig. 4a. In Fig. 4b, the Mn 2p spectrum displays binding energy peaks at 641.25 eV (Mn 2p3/2) and 653.16 eV (Mn 2p1/2), with a peak separation of 11.91 eV. Fig. 4c presents the Mn 3s spectrum, which exhibits two low binding energy peaks at 82.62 eV and 88.64 eV, with a peak difference of 5.71 eV. Furthermore, the O 1s XPS spectrum [Fig. 4d] is observed at around 532 eV, confirming the presence of oxygen in the sample. The observed binding energy differences between the Mn 3s and Mn 2p peaks are consistent with previous reports [25].

For the Co_3O_4 sample, Figure 4e shows the Co 2p spectrum, which exhibits peak splitting at 780 eV (Co 2p3/2) and 795 eV (Co 2p1/2) with a peak separation of 15 eV [28]. This spectrum confirms the presence of cobalt and its chemical state in the Co_3O_4 nanocrystals.

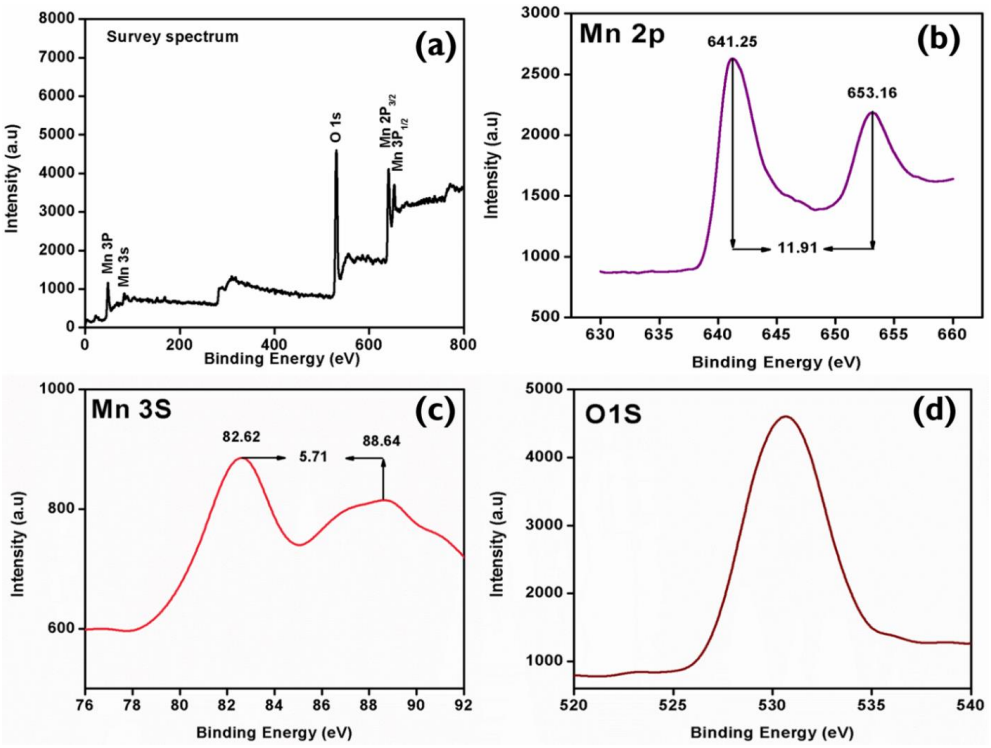

Figure 4: XPS spectra of Mn_3O_4 nanocrystals: (a) Survey spectrum, (b) Mn 2p (c) Mn 3s and (d) O 1s.

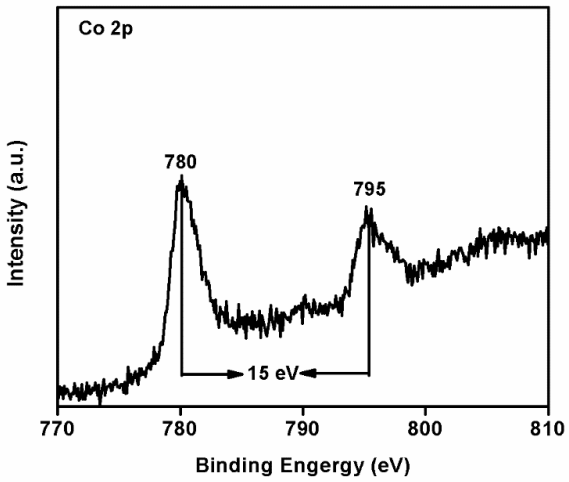

Figure 4: (e) XPS spectra of Co_3O_4 nanocrystals

B. Optical and Magnetic properties

UV-Vis spectroscopy was employed to study the optical properties of the synthesized nanocrystals in the wavelength range of 300-1000 nm, aiming to estimate their optical band gap. The resulting optical band gap spectra, along with the absorption spectra (inset of Fig. 5), were observed. The nanocrystals exhibited a p-type semiconductor nature and displayed notable absorption in the visible region. By utilizing the appropriate formula [29], the calculated optical band gap values for Mn_3O_4 and Co_3O_4 nanocrystals were found to be 2.93 eV and 2.5 eV, respectively.

It is noteworthy that the determined Eg values for Mn_3O_4 and Co_3O_4 nanocrystals in our study are higher than those reported in previous research [30]. This increase in the band gap is attributed to the quantum confinement effects and the presence of oxygen vacancies within the Mn_3O_4 and Co_3O_4 nanoparticles [31-34]. These factors influence the electronic structure and energy levels, leading to an elevated optical band gap in the synthesized nanocrystals

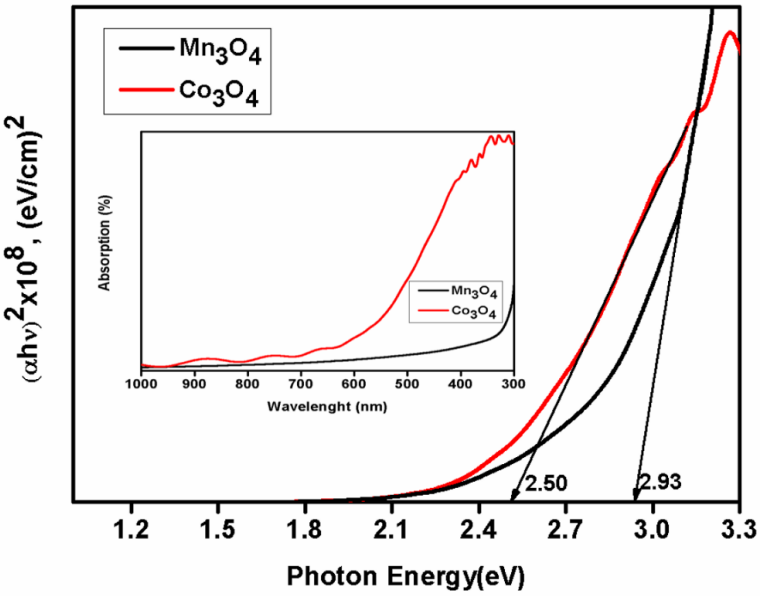

Figure 5: Optical band gap of spinel Mn_3O_4 and Co_3O_4 nanocrystals

The magnetic properties of Mn_3O_4 and Co_3O_4 nanocrystals were investigated using Vibrating Sample Magnetometer (VSM) over a temperature range of 5 K to 300 K, as shown in Fig. 6. The magnetic behavior of complex oxides like Mn_3O_4 and Co_3O_4, with normal spinel structures, is known to strongly depend on the oxygen content. In our study, the oxygen stoichiometry of the prepared Mn_3O_4 and Co_3O_4 nanocrystals was determined to be $Mn_3O_{4.06}$ and $Co_3O_{3.9}$, respectively, indicating oxygen excess and deficit in the respective samples. The stoichiometric Mn3O4.06 sample exhibited ferromagnetic properties, as shown in Fig. 6a&b, with the magnetization curve at 5 K displaying a hysteresis loop characteristic of ferromagnetism. At 300 K, the curve resembled paramagnetic behavior.

The average oxidation level of manganese cations in the octahedral coordination of oxygen cations was found to be predominantly Mn^{3+} (70.9%) with a lesser percentage of Mn^{4+} (19.1%). The remanence magnetization (Mr) and coercivity (Hc) values were determined to be 0.199 emu/g and 1.06 kOe, respectively, for the $Mn_3O_{4.06}$ sample.

On the other hand, the $Co_3O_{3.9}$ sample displayed weak ferromagnetic properties, as shown in Fig. 6c&d, with a saturation magnetization value of 0.25 emu/g at an applied magnetic field of 0.7 kOe. The change from an antiferromagnetic state in bulk Co_3O_4 to a weakly ferromagnetic state in the $Co_3O_{3.9}$ nanocrystals can be attributed to uncompensated surface spins and/or finite size effects. The magnetic properties of nanomaterials are known to strongly depend on particle shape, size, crystallinity, and magnetization direction. The Co3O3.9 sample can be regarded as a ferromagnetic matrix containing antiferromagnetic clusters due to the appearance of oxygen vacancies, resulting in antiferromagnetic interactions.

In conclusion, the magnetic behavior of Mn_3O_4 and Co_3O_4 nanocrystals is influenced by oxygen stoichiometry and the presence of oxygen vacancies, leading to ferromagnetic and weak ferromagnetic properties, respectively. The competition between antiferromagnetic and ferromagnetic interactions results in the formation of the spin glass state in $Co_3O_{3.9}$ nanocrystals.

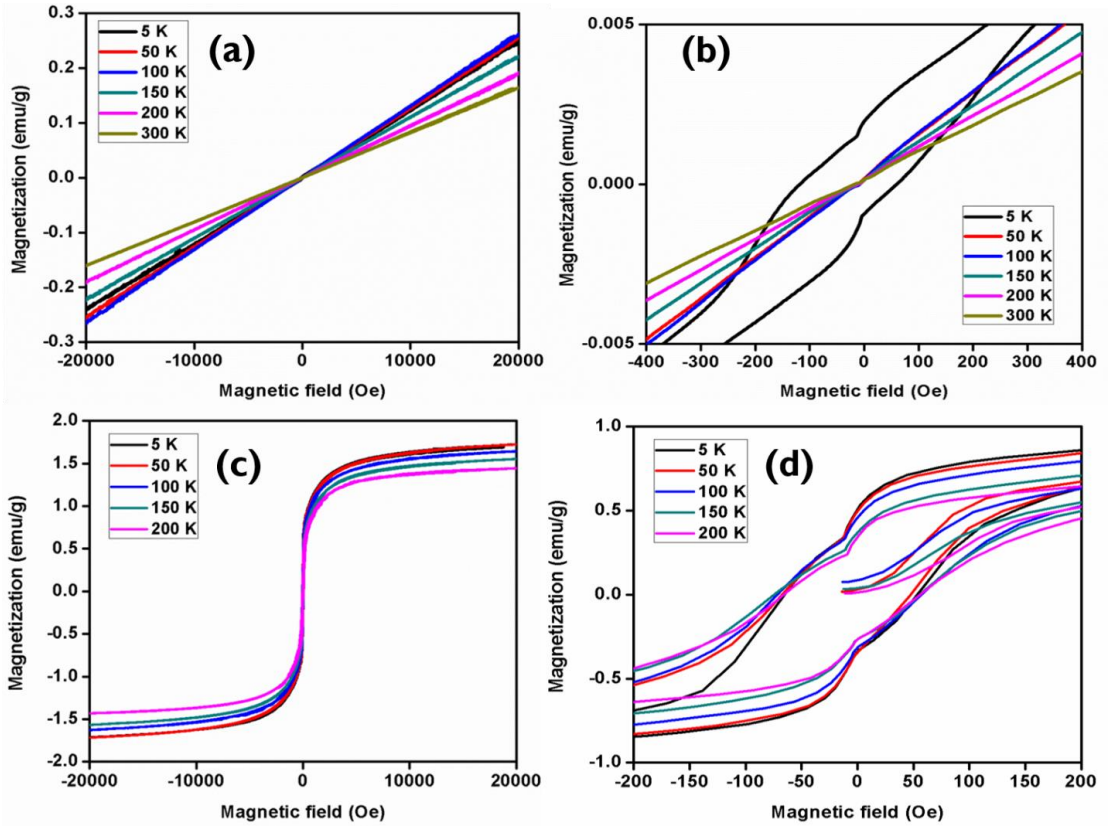

Figure 6: The M–H curves of Mn_3O_4(a & b) and Co_3O_4 (c & d) nanocrystals at 5K to 300 K.

C. Dielectric properties

The capacitive behavior of the $Mn_3O_{4.06}$ sample is analyzed using frequency and potential dependence of capacitance curves, as depicted in Fig. 7a and 7b. Fig. 7a shows that the capacitance is higher at lower frequencies and decreases as the frequency increases, eventually reaching a constant value at higher frequencies. The high capacitance at lower frequencies can be attributed to the presence of space charge polarization, which diminishes with increasing frequency, leading to a frequency-independent behavior at higher frequencies. Moreover, the capacitance of the sample is observed to increase with temperature, as studied at different temperatures ranging from 313 K to 373 K.

Furthermore, the change in capacitance of the $Mn_3O_{4.06}$ sample with potential at various temperatures is investigated, as shown in Fig. 7b. It is found that the decrease in oxygen vacancies leads to an increase in the conductivity of the sample, resulting in superior electrochemical properties [36].

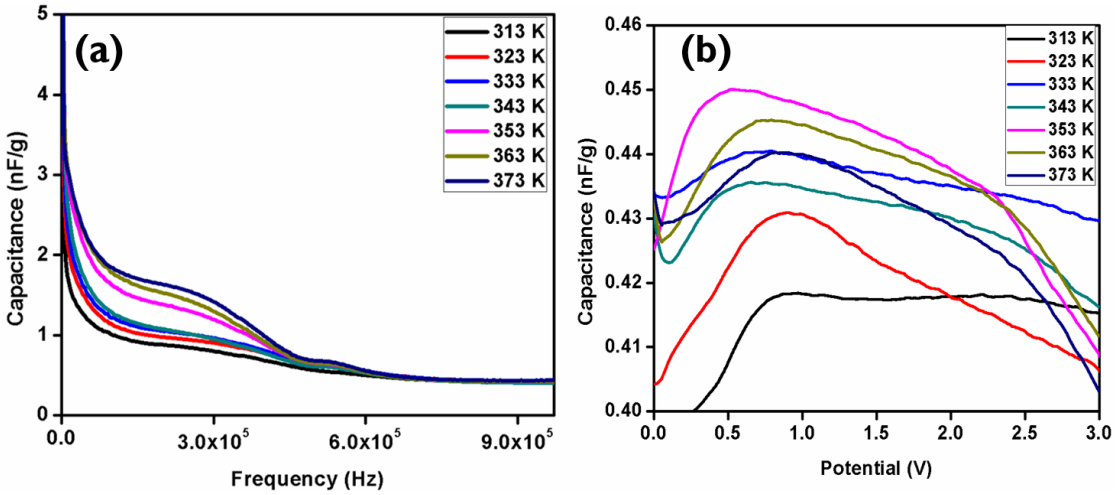

Figure 7: (a) Dependence of AC capacitance on frequency b) capacitance on potential of Mn_3O_4 nanocrystals

D. Electrochemical properties

The Cyclic Voltammetry (CV) studies of the nanocrystals were conducted in a 1M Na_2SO_4 aqueous solution at different scan rates: 1-50 mVs-1 for Mn3O4 and 1-10 mVs-1 for Co3O4, with potential window ranges of -0.1 V to +0.9 V (Mn_3O_4) and -0.1 V to 0.7 V (Co_3O_4), respectively. As shown in Fig. 8a&b, the CV curves exhibit a rectangular and semi-rectangular shape without any redox peaks, indicating the presence of interface capacitance between the electrode and the electrolyte. It was observed that the area under the curves increases with the scan rate; however, the specific capacitance decreases due to the limitation of electrolytic ions to the electrode surface at higher scan rates. Nevertheless, the shape of the CV curves remains consistent, indicating the chemical stability of the sample. The specific capacitance (C) of the samples at various scan rates was calculated using equation (2) and the values are presented in Table 1 [25, 38, 39].

Cyclic Voltammetry (CV) studies of nanocrystals are investigated in 1M Na_2SO_4 aqueous solution at different scan rates from 1- 50 mVs^{-1} (Mn_3O_4) and 1-10 mVs^{-1} (Co_3O_4) in the potential window range -0.1 V to +0.9 V (Mn_3O_4) and -0.1 to 0.7 V (Co_3O_4), respectively. Fig. 8 a & b show the rectangular and semi rectangular shape of CV curves without any redox peaks indicating the interface capacitance between electrode and electrolyte. Although the area under the curves is increased with scan rate, the specific capacitance is decreased because the electrolytic ions are limited to the electrode surface at higher scan rate. At the same time, the shape of the CV curves remains same which indicates the chemical stability of the sample. The specific capacitance (C) of the samples at various scan rates measured by the following equation (2) and their values are displayed in Table 1. [25, 38, 39].

$$C = \frac{\int I(V)\,dV}{(2m\,\Delta V\,(V_2 - V_1))} \qquad \text{---} \qquad (2)$$

where, $\int I(V)\,dV$ = total voltammetric charge in coulomb, , m = mass of the active electrode in gram, , ΔV = scan rate in Vs^{-1} and $(V_2 - V_1)$ = potential window range in V. In Table 1, the specific capacitance values decrease with an increase in the scan rate. This observation is attributed to the fact that at lower scan rates, there is sufficient time for the electrolyte ions to occupy almost all the active sites of the electrode material, resulting in higher specific capacitance. Conversely, at higher scan rates, the limited time available for the electrolyte ions to reach the electrode surface leads to a lower specific capacitance.

The capacitive nature of the samples is further evident from the Chronopotentiometry studies. The charge-discharge cycles of the samples at various current densities are shown in Fig. 8c & d. The Mn_3O_4 nanocrystals exhibit symmetric charge-discharge curves, indicating high electrochemical reversibility and excellent capacitive behavior, which corroborates the CV results. On the other hand, the charge-discharge curves of the Co_3O_4 nanocrystals are asymmetric, with lower discharging time. The discharge capacitance (C) was calculated using the following equation (3) [25].

$$C = \frac{I\,\Delta t}{\Delta V\, m} \qquad \text{---} \qquad (3)$$

where, I= current in ampere, Δt = discharge time in second, , V= potential window in volt and m= mass of active electrode material in gram. The Mn_3O_4 and Co_3O_4 nanocrystals demonstrated distinct discharge capacitance values at 0.5 Ag-1 current density, reaching 417 and 214 Fg-1, respectively. These specific capacitance values were calculated and listed in Table 2 for various current densities. The results from the constant potential (CP) studies aligned with the cyclic voltammetry (CV) findings.

A critical factor in supercapacitors is their long-term cyclic stability. To assess this, the Mn3O4 charge-discharge cycles were conducted for 10000 cycles at a current density of 2 Ag-1 (Fig. 8e). Remarkably, even after 10000 cycles, 81% of capacitive retention was observed. In contrast, Co3O4 exhibited 70% capacitive retention at 0.5 Ag-1 current density (Fig. 8g). The charge-discharge curves of Mn3O4 displayed a symmetric pattern with cycle number, indicating a high level of electrochemical reversibility and excellent capacitive behavior [40-44]. The coulombic efficiency was calculated using formula (4).

$$\eta = \frac{t_d}{t_c} \times 100 \qquad \text{---} \qquad (4)$$

where, η, t_d and t_c refers to coulombic efficienty, discharge time and charging time respectively. The Mn_3O_4 electrode exhibited 100% coulombic efficiency after 600 cycles as shown in Figure 8e.

Electrochemical Impedance Spectroscopy (EIS) is another characterization technique employed to investigate the capacitive behavior of the electrode materials. EIS analysis of the sample is conducted in the frequency range from 1 Hz to 1 MHz to corroborate the CV results. The Nyquist plots of the Mn3O4 nanoparticles are shown in Fig. 8f. The intersection of the Nyquist plots on the real axis at higher frequencies represents the solution resistance (RS). It is observed that both the solution and charge transfer resistances of the materials are smaller before cycling and become higher after 10,000 cycles, which leads to a decrease in specific capacitance with the number of cycles, as depicted in Fig. 8f&h.

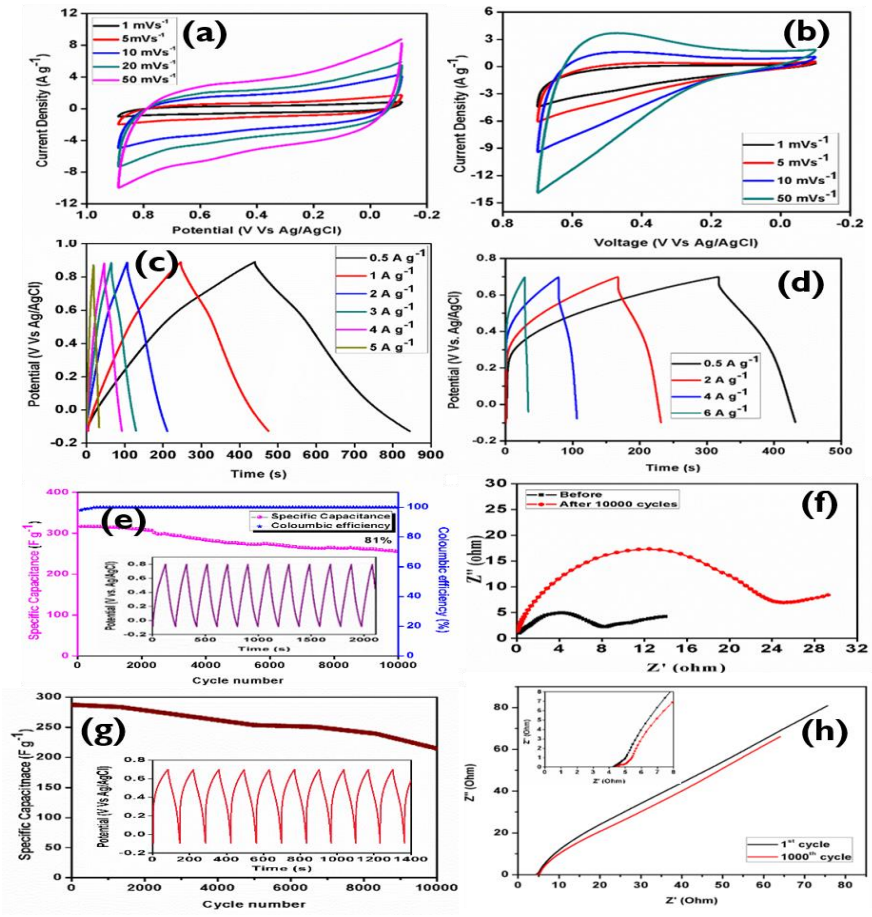

Figure 8: a) CV curves of spinel Mn_3O_4 and b) Co_3O_4 nanocrystals at different scan rates. c) Charge-discharge curves of spinel Mn_3O_4 and d) Co_3O_4 nanocrystals at different scan rates e) Specific capacitance and coloumbic efficiency with cycle number f) Nyquist plots of Mn_3O_4 nanocrystals g) Specific capacitance with cycle number h) Nyquist plots of Co_3O_4 nanocrystals.

IV. CONCLUSION

The spinel nanostructures of Mn_3O_4 and Co_3O_4 were successfully synthesized using the solution combustion technique. XRD and Raman studies confirmed the establishment of tetragonal Mn_3O_4 and cubic Co_3O_4 structures, with estimated crystallite sizes of 14 nm and 22 nm, respectively. FTIR measurements further supported the formation of manganese oxide and cobalt oxide, evident from the presence of Mn-O and Co-O bonding. The SEM micrographs showed dispersed irregular grains of approximately 100 nm size for Mn_3O_4 and uniformly distributed spherical grains with an average size of 120 nm for Co_3O_4. The optical band gaps of the samples were measured to be 2.93 eV for Mn_3O_4 and 2.50 eV for Co_3O_4 nanocrystals. Additionally, the magnetic properties of both samples exhibited strong ferromagnetic behavior at around 5 K temperature. The electrochemical characterization studies, including CV, Chronopotentiometry, and EIS, were performed in 1M Na_2SO_4 aqueous electrolyte. The as-prepared Mn_3O_4 nanocrystals demonstrated the highest specific capacitance of 417 F g^{-1} at a current density of 0.5 A g^{-1}, along with good cyclic stability and almost 100% coulombic efficiency. Based on these results, it can be concluded that nanocrystalline Mn_3O_4 holds promise as an excellent electrode material for supercapacitor applications.

REFERENCES

[1]. P Suktha, N Phattharasupakun, P Dittanet and M Sawangphruk "Charge storage mechanisms of electrospun Mn_3O_4 nanofibres for high-performance supercapacitors" RSC Adv., 7 (2017) 9958-9963.

[2]. J. Chmiola , G. Yushin , Y. Gogotsi , C. Portet , P. Simon and P. L. Taberna "Anomalous Increase in Carbon Capacitance at Pore Sizes Less Than 1 Nanometer" Science, 313 (2006) 1760 —1763.

[3]. P. Huang , C. Lethien , S. Pinaud , K. Brousse , R. Laloo , V. Turq , M. Respaud , A. Demortière , B. Daffos , P. L. Taberna , B. Chaudret , Y. Gogotsi and P. Simon "On-chip and freestanding elastic carbon films for micro-supercapacitors" Science, 351 (2016) 691 — 695.

[4]. D. Pech , M. Brunet , H. Durou , P. Huang , V. Mochalin , Y. Gogotsi , P.-L. Taberna and P. Simon "Ultrahigh-power micrometre-sized supercapacitors based on onion-like carbon" Nat. Nanotechnol., 5 (2010) 651 — 654.

[5]. P Naresh Kumar Reddy, Dadamiah PMD Shaik, Vattikondala Ganesh, D Nagamalleswari, K Thyagarajan, P Vishnu Prasanth "Structural, optical and electrochemical properties of TiO2 nanoparticles synthesized using medicinal plant leaf extract" Ceramics International. 45 (2019) 16251-16260

[6]. B. G. S. Raj , R. N. R. Ramprasad , A. M. Asiri , J. J. Wu and S. Anandan "Ultrasound assisted synthesis of Mn_3O_4 nanoparticles anchored graphene nanosheets for supercapacitor applications" Electrochim. Acta, 156 (2015) 127 —137.

[7]. L. Yang , S. Cheng , X. Ji , Y. Jiang , J. Zhou and M. Liu "Investigations into the origin of pseudocapacitive behavior of Mn_3O_4 electrodes using in operando Raman spectroscopy" J. Mater. Chem. A 3 (2015) 7338 —7344.

[8]. G. S. Gund , D. P. Dubal , B. H. Patil , S. S. Shinde and C. D. Lokhande "Enhanced activity of chemically synthesized hybrid graphene oxide/Mn_3O_4 composite for high performance supercapacitors" Electrochim. Acta 92 (2013) 205 —215.

[9]. C.-H. Yang , I. W. Sun , C.-T. Hsieh , T.-Y. Wu , C.-Y. Su , Y.-S. Li and J.-K. Chang "Facile electrochemical preparation of hierarchical porous structures to enhance manganese oxide charge-storage properties in ionic liquid electrolytes" J. Mater. Chem. A 4 (2016) 4015 —4018.

[10]. M.-J. Deng , P.-J. Ho , C.-Z. Song , S.-A. Chen , J.-F. Lee , J.-M. Chen and K.-T. Lu "Fabrication of Mn/Mn oxide core–shell electrodes with three-dimensionally ordered macroporous structures for high-capacitance supercapacitors" Energy Environ. Sci. 6 (2013) 2178 —2185.

[11]. M.-J. Deng , J.-K. Chang , C.-C. Wang , K.-W. Chen , C.-M. Lin , M.-T. Tang , J.-M. Chen and K.-T. Lu "High-performance electrochemical pseudo-capacitor based on MnO_2 nanowires/Ni foam as electrode with a novel Li-ion quasi-ionic liquid as electrolyte" Energy Environ. Sci. 4 (2011) 3942 —3946.

[12]. T. Ngoc, T. Pham and Y S Yoon "Development of Nanosized Mn_3O_4-Co_3O_4 on Multiwalled Carbon Nanotubes for Cathode catalyst in urea fuel cell" Energies 13 (2020) 2322-2335

[13]. R. Regmi, R. Tackett, G. Lawes Journal of Magnetism and Magnetic Mateirals "Suppression of low-temperature magnetic states in Mn_3O_4 nanoparticles" 321 (2009) 2296-2299.

[14]. Vipin C. Bose, V. Biju, "Optical, electrical and magnetic properties of nanostructured Mn_3O_4 synthesized through a facile chemical route" Physica E, 66(2015) 24–32.

[15]. M.A. Almessiere, A.V. Trukhanov, F.A. Khan, Y. Slimani, N. Tashkandi, V.A. Turchenko, T.I. Zubar, D.I. Tishkevich, S.V. Trukhanov, L.V. Panina, A. Baykal, Correlation between microstructure parameters and anti-cancer activity of the $[Mn_{0.5}Zn_{0.5}](Eu_xNdxFe_{2-2x})O_4$ nanoferrites produced by modified sol-gel and ultrasonic methods, Ceram. Int. 46 (2020) 7346-7354.

[16]. M.A. Almessiere, Y. Slimani, H. Güngüneş, V.G. Kostishyn, S.V. Trukhanov, A.V. Trukhanov, A. Baykal, Impact of Eu3+ ion substitution on structural, magnetic and microwave traits of Ni-Cu-Zn spinel ferrites, Ceram. Int. 46 (2020) 11124-11131.

[17]. D.A. Vinnik, F.V. Podgornov, N.S. Zabeivorota, E.A. Trofimov, V.E. Zhivulin, A.S. Chernukha, M.V. Gavrilyak, S.A. Gudkova, D.A. Zherebtsov, A.V. Ryabov, S.V. Trukhanov, T.I. Zubar, L.V. Panina, S.V. Podgornaya, M.V. Zdorovets, A.V. Trukhanov, Effect of treatment conditions on structure and magnetodielectric properties of barium hexaferrites, J. Magn. Magn. Mater. 498 (2020) 166190.

[18]. A.L. Kozlovskiy, I.E. Kenzhina, M.V. Zdorovets, FeCo-Fe2CoO4/Co3O4 nanocomposites: Phase transformations as a result of thermal annealing and practical application in catalysis, Ceram. Int. 46 (2020) 10262-10269.

[19]. K. Dukenbayev, I.V. Korolkov, D.I. Tishkevich, A.L. Kozlovskiy, S.V. Trukhanov, Y.G. Gorin, E.E. Shumskaya, E.Y. Kaniukov, D.A. Vinnik, M.V. Zdorovets, M. Anisovich, A.V. Trukhanov, D. Tosi, C. Molardi, Fe3O4 nanoparticles for complex targeted delivery and boron neutron capture therapy, Nanomaterials-Basel 9 (2019) 494.

[20]. D.I. Tishkevich, I.V. Korolkov, A.L. Kozlovskiy, M. Anisovich, D.A. Vinnik, A.E. Ermekova, A.I. Vorobjova, E.E. Shumskaya, T.I. Zubar, S.V. Trukhanov, M.V. Zdorovets, A.V. Trukhanov, Immobilization of boron-rich compound on Fe3O4 nanoparticles: Stability and cytotoxicity, J. Alloys Compd. 797 (2019) 573-581.

[21]. M.A. Almessiere, A.V. Trukhanov, Y. Slimani, K.Y. You, S.V. Trukhanov, E.L. Trukhanova, F. Esa, A. Sadaqat, K. Chaudhary, M. Zdorovets, A. Baykal, Correlation between composition and electrodynamics properties in nanocomposites based on hard/soft ferrimagnetics with strong exchange coupling, Nanomaterials-Basel 9 (2019) 202.

[22]. M.V. Zdorovets, A.L. Kozlovskiy, Study of phase transformations in Co/CoCo2O4 nanowires, J. Alloys Compd, 815 (2020) 152450.

[23]. Lorenzo Bigiani, Mariam Hassan, Davide Peddis, Chiara Maccato, Gaspare Varvaro, Cinzia Sada, Elza Bontempi, Sara Martí-Sanchez, Jordi Arbiol and Davide Barreca, High Magnetic Coercivity in Nanostructured Mn_3O_4 Thin Films Obtained by Chemical Vapor Deposition. DOI: 10.1021/acsanm.9b00141

[24]. A.D. Khalajia, M. Soleymanifarda M. Jarosovab and P. Machek, Facile Synthesis and Characterization of Mn_3O_4, Co_3O_4, and NiO, Acta Physica Polonica A, 6 137 (2020), 1043-1045

[25]. Dadamiah PMD Shaik, P. Rosaiah, Y Qiu and O. M. Hussain, "Hydrothermally synthesized porous Mn_3O_4 nanoparticles with enhanced electrochemical performance for supercapacitors" Ceramics International, 45(2) (2019), 2226-2233.

[26]. N. Mironova-Ulmanea, A. Kuzmina, V. Skvortsova, G. Chikvaidze, I. Sildos, J. Grabisc, D. Jankovi, A. Dindune and M. Maiorov, Synthesis and Vibration Spectroscopy of Nano-Sized Manganese Oxides, Acta Physica Polonica A, 4 133 2018 1013-1016.

[27]. Saeed Farhadi, Masoumeh Javanmard and Gholamali Nadri, Characterization of Cobalt Oxide Nanoparticles Prepared by the Thermal Decomposition of $[Co(NH_3)_5(H_2O)](NO_3)_3$ Complex and Study of Their Photocatalytic Activity

[28]. Thi Ngoc Tuyen Pham and Young Soo Yoon" Development of Nanosized Mn_3O_4-Co_3O_4 on Multiwalled Carbon Nanotubes for Cathode Catalyst in Urea Fuel Cell" Energies 2020, 13, 2322, Energies 2020, 13, 2322

[29]. SubhashThota, AshokKumar, JitendraKumar "Optical, electrical and magnetic properties of Co_3O_4 nanocrystallites obtained by thermal decomposition of sol–gel derived oxalates" 164 (2009) 30-37.

[30]. Saeed Farhadi, Jalil Safabakhsh and Parisa Zaringhadam, Synthesis, characterization, and investigation of optical and magnetic properties of cobalt oxide (Co_3O_4) nanoparticles. Journal Of Nanostructure in Chemistry1-9.

[31]. S.V. Trukhanov, I.O. Troyanchuk, N.V. Pushkarev, H. Szymczak, The influence of oxygen deficiency on the magnetic and electric properties of La0.70Ba0.30MnO3-γ ($0 \leq \gamma \leq 0.30$) manganite with a perovskite structure, JETP 95 (2002) 308-315.

[32]. I.Z. Zhumatayeva, I.E. Kenzhina, A.L. Kozlovskiy, M.V. Zdorovets, The study of the prospects for the use of Li0.15Sr0.85TiO3 ceramics, J. Mater. Sci.: Mater. Electron. 31 (2020) 6764–6772.

[33]. S.V. Trukhanov, V.A. Khomchenko, L.S. Lobanovski, M.V. Bushinsky, D.V. Karpinsky, V.V. Fedotova, I.O. Troyanchuk, A.V. Trukhanov, S.G. Stepin, R. Szymczak, C.E. Botez, A. Adair, Crystal structure and magnetic properties of Ba-ordered manganites Ln0.70Ba0.30MnO3−δ (Ln = Pr, Nd), JETP 103 (2006) 398–410.

[34]. K.K. Kadyrzhanov, D.I. Shlimas, A.L. Kozlovskiy, M.V. Zdorovets, Research of the shielding effect and radiation resistance of composite CuBi2O4 films as well as their practical applications. J. Mater. Sci.: Mater. Electron. 31 (2020) 11729–11740.

[35]. S. Fritsch, J. Sarrais, A. Rousset and G.U. Kulkarni "Low-temperature oxidation of Mn3O4 Hausmannite" Materials Research Bulletin, 33 (1998) 1185-1194.
[36]. I.O. Troyanchuk, S.V. Trukhanov, D.D. Khalyavin, H. Szymczak, Magnetic properties of anion deficit manganites Ln0.55Ba0.45MnO3-γ (Ln=La, Nd, Sm, Gd, $\gamma \leqslant 0.37$), J. Magn. Magn. Mater. 208 (2000) 217-220.

[37]. S.V. Trukhanov, A.V. Trukhanov, A.N. Vasil'ev, A. Maignan, H. Szymczak, Critical behavior of La0.825Sr0.175MnO2.912 anion-deficient manganite in the magnetic phase transition region, JETP Lett. 85 (2007) 507-512.

[38]. Vijaya Sankar K, Kalpana D, Kalai Selvan R " Electrochemical Properties of microwave-assisted reflux-synthesized Mn_3O_4 nanoparticles in different electrolytes for supercapacitor applications" Journal of Applied Electrochemistry 42 (2012) 463-470.
[39]. Lu-Feng Y, Chuang G, Ming-Tao Z, Chao-Fan H, Jiang-Hu C, Ying-Liang L "Synthesis and Electrochemical properties of Mn_3O_4 polyhedral nanocrystals" Chinese Journal of Inorganic Chemistry 29(2013) 381-388.
[40]. H. Jiang, T. Zhao, C.Y. Yan, J. Ma, C. Z. Li " Hydrothemal synthesis of novel Mn_3O_4 nano-octahedrons with enhanced supercapacitors performances" Nanoscale 2 (2010) 2195-2198
[41]. Ghodbane O, Pascal J L, Fraisse B, Favier F. "Structural in situ study of the Thermal behavior of Manganese dioxide material:Toward selected electrode materials for supercapacitors" ACS applied materials and Interfaces 2 (2010) 3493-3505
[42]. H. Jiang, T. Zhao, C.Y. Yan, J. Ma, C. Z. Li "High–rate electrochemical capacitors from highly graphitic carbon–tipped manganese oxide/mesoporous carbon/manganese oxide hybrid nanowires" Nanoscale 2, 2195 (2010)
[43]. CM Julien, M. Massot, C. Poinsignon "Lattice vibrations of manganese oxides. Part I. Periodic structures" Spectrochimica Acta A 60(2004) 689-700
[44]. Shuang-Yu Liu, Jian Xie, Yun-Xiao Zheng, Gao-Shao Cao, Tie-Jun Zhu, Xin-Bing Zhao "Nanocrystal manganese oxide (Mn_3O_4, MnO) anchored on graphite nanosheet with improved electrochemical Li-storage properties" Electrochimica Acta 66 (2012) 271-278.